

Realistic analytical approach for α decay and clusteringD. S. Delion^{1,2,3} and A. Dumitrescu^{1,2}¹*Horia Hulubei National Institute for R&D in Physics and Nuclear Engineering,
P. O. Box MG-6, RO-077125, Bucharest-Măgurele, România*²*Academy of Romanian Scientists, 54 Splaiul Independenței RO-050085, Bucharest, România*³*Bioterra University, 81 Gârlei RO-013724, Bucharest, România*

(Received 23 April 2020; accepted 15 July 2020; published 29 July 2020)

We approximate the realistic α -core nuclear interaction between the inner turning point and Coulomb barrier, derived within the double folding procedure, by a parabolic dependence. It turns out that the corresponding harmonic oscillator frequency is concentrated in a narrow interval around $\hbar\omega_1 \approx 9$ MeV for all analyzed transitions from even-even and odd-mass α emitters. The penetrability through the nuclear barrier has an exponential dependence on the ratio between the fragmentation potential and this harmonic oscillator frequency. On the other hand, the Coulomb penetrability has the standard dependence on the Coulomb parameter. Our analysis revealed that the reduced width, extracted by using the nuclear plus Coulomb penetrability factors, exponentially decreases versus the number of α clusters along all analyzed α lines, except one region where it increases by approaching the neutron magic number $N_{\text{mag}} = 126$. In that case, the number of valence proton pairs is much smaller than the number of valence neutron pairs. The reduced width exponentially depends on the magic neutron-proton asymmetry above doubly magic nuclei. These dependencies allow us to propose a systematics for reduced widths in terms of the quartet number and magic asymmetry evaluated above the closest doubly magic nuclei.

DOI: [10.1103/PhysRevC.102.014327](https://doi.org/10.1103/PhysRevC.102.014327)**I. INTRODUCTION**

The α -particle has a large binding energy/nucleon and therefore it survives as a basic building block in the structure of light nuclei [1,2]. A striking example is given by quasimolecular rotational bands in light nuclei [3]. These states naturally occur in a quasimolecular pocketlike α -core potential, with a minimum in the nuclear surface region. The importance of α clustering in the nuclear structure above doubly magic nuclei was stressed not only for light but also for heavy systems [4–6]. On the other hand, the strong α clustering feature is revealed by decaying nuclei with $Z \geq 50$. In the early years of quantum mechanics this process was interpreted as a penetration of “preformed” α clusters through the Coulomb barrier [7,8]. The later attempts to explain the α formation in terms of two proton and two neutron single-particle orbitals, generated by the nuclear mean field, failed [9,10]. It is a well-established fact that the α -decay width cannot be described without an important clustering component mixed with standard shell orbitals [11]. It turns out that the four-body correlations are enhanced in the surface region and this can be simulated by adding a Gaussian component on top of the standard nuclear mean field [12]. Thus, α -like configurations are favored at small densities beyond the nuclear surface, due to the fact that the Pauli principle prohibits their existence inside nuclei [13,14]. This leads to a quasimolecular pocketlike α -core interaction, centered on the nuclear surface, explaining the systematics of the decay width between ground states [15]. A very significant result concerning the quasi-

molecular interpretation of the α -daughter rotating configurations is given in Ref. [16]. Namely, the strength of the α -daughter quadrupole-quadrupole interaction reproducing the experimental widths to 2^+ states in even-even nuclei is larger above magic nuclei and linearly decreases by adding α -cluster configurations. Therefore, the spectroscopic factor also has larger values above magic numbers, thus revealing a rotating α -daughter molecular $[L^+ \otimes L^+]_0$ configuration with a large probability.

The first goal of this paper is to give a simple analytical approach for the α -core interaction by analyzing its realistic shape provided within the double-folding procedure. The second goal is to use the parameters of this potential in order to extract the penetration factor through the nuclear plus Coulomb barrier and to analyze the remaining reduced width in terms of α clusters plus the excess neutron pairs on top of a doubly magic nucleus. The paper is organized as follows: In Sec. II we give theoretical details concerning the α -core potential and reduced decay width, and in Sec. III we analyze potential parameters and α -decay data. In the last section we draw conclusions.

II. THEORETICAL BACKGROUND

The two-body dynamics of composite objects, like the α -daughter system, is described within the resonating group method (RGM). It accounts exactly for the Pauli exchange effects, leading to the occurrence of a repulsive core in the Hamiltonian kernel [17,18]. However, an effective pocketlike

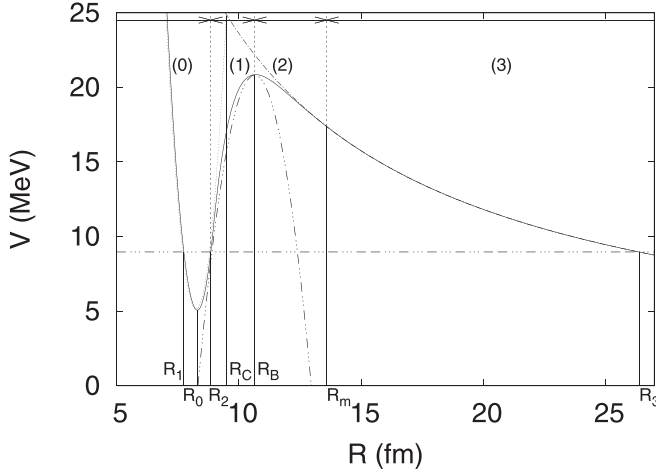


FIG. 1. Realistic α -daughter double-folding plus ho repulsive potential versus radius for the system $^{208}\text{Pb} + \alpha$, plotted by a solid line. The repulsive ho part is plotted by dots, the parabolic approximation of the double folding interaction by triple dot-dashes, and the pure Coulomb potential by a dot-dashed line. The horizontal line corresponds to the Q value of the emission process $^{212}\text{Po} \rightarrow ^{208}\text{Pb} + \alpha$.

local potential simulating the Pauli principle for α decay can be introduced to analyze data in a simpler way [19].

A. Interaction potential

We will investigate α transitions $P(J_P) \rightarrow D(J_D) + \alpha(l)$, where $J_{P/D}$ is the short-hand notation for the spin^{parity} of the parent/daughter nucleus. The wave function, describing the relative α -core dynamics, can be expanded as follows:

$$\Psi(\mathbf{R}) = \sum_{l=|J_P-J_D|}^{J_P+J_D} \frac{f_l(R)}{R} Y_{lm}(\hat{\mathbf{R}}), \quad (2.1)$$

where $\mathbf{R} = (R, \hat{\mathbf{R}})$ denotes the α -core distance. Each radial partial wave satisfies the stationary Schrödinger equation,

$$\left[-\frac{d^2}{d\rho^2} + \frac{V_l(R)}{Q} - 1 \right] f_l(R) = 0$$

$$\frac{V_l(R)}{Q} \equiv \frac{l(l+1)}{\rho^2} + \frac{V(R)}{Q}, \quad (2.2)$$

written in terms of the reduced radius

$$\rho = \kappa R, \quad \kappa = \mu_\alpha v / \hbar, \quad (2.3)$$

where μ_α is the reduced mass of the α -core system, Q denotes the energy release of the process (Q value), and $v = \sqrt{2Q/\mu_\alpha}$ is the asymptotic velocity.

Recently, we have shown in Ref. [20] that the α emission process is described by a shifted harmonic oscillator (ho) quasimolecular potential matched to a realistic double folding interaction [21–23]. This potential is plotted in Fig. 1 by a solid line for the emission process $^{212}\text{Po} \rightarrow ^{208}\text{Pb} + \alpha$. A very good approximation of this interaction is given by the

following ansatz:

$$V(R) = V_0 + \frac{1}{2} \hbar \omega_0 \beta_0 (R - R_0)^2, \quad R \leq R_2, \quad (0)$$

$$= V_B - \frac{1}{2} \hbar \omega_1 \beta_1 (R - R_B)^2, \quad R_2 < R \leq R_B, \quad (1)$$

$$= V_B - a \left(\frac{R}{R_B} - 1 \right)^2, \quad R_B < R \leq R_m, \quad (2)$$

$$= V_C(R) \equiv \frac{ZZ_\alpha e^2}{R}, \quad R > R_m, \quad (3) \quad (2.4)$$

where $\hbar \omega_k$ denote ho frequencies, a is the strength of the potential in the transitional region, Z is the charge of the daughter nucleus, and R_2 is the second turning point, i.e., the second solution of the equation $V(R) = Q$.

We obtained the following rule for the barrier height in terms of the Coulomb potential:

$$V_B \approx 0.939 V_C(R_B), \quad \sigma = 0.003. \quad (2.5)$$

The ho parameters of the two parabolas are defined as follows:

$$\beta_k = \frac{\mu_\alpha \omega_k}{\hbar} = \frac{1}{b_k^2} \equiv d_\alpha \hbar \omega_k, \quad k = 0, 1, \quad (2.6)$$

where b_k define ho size parameters. Notice that for heavy α emitters $\mu_\alpha \approx 4M_N$ and one obtains

$$d_\alpha = \frac{\mu_\alpha c^2}{(\hbar c)^2} \approx 0.096 \text{ MeV}^{-1} \text{ fm}^{-2}. \quad (2.7)$$

From Eq. (2.4) it is obvious that our potential is continuous at the barrier radius R_B . We use the continuity between functions and derivatives at R_m connecting the regions (2) and (3) in order to obtain

$$R_m = \frac{3}{4} \frac{V_C(R_B)}{V_B} \left[1 + \sqrt{1 - \frac{8}{9} \frac{V_B}{V_C(R_B)}} \right] R_B \approx 1.123 R_B$$

$$a = \frac{V_B - V_C(R_c)}{(R_c/R_B - 1)^2} \approx 3.208 V_C(R_B). \quad (2.8)$$

We will show in the next subsection that the wave function in the region (2) can be approximated by the standard Wentzel-Kramer-Brillouin (WKB) semiclassical ansatz for a pure Coulomb potential.

In region (3), defining the pure Coulomb interaction, the Schrödinger equation (2.2) acquires the following form:

$$\left[-\frac{d^2}{d\rho^2} + \frac{l(l+1)}{\rho^2} + \frac{\chi}{\rho} - 1 \right] f_l(R) = 0, \quad (2.9)$$

depending on the Coulomb parameter,

$$\chi = \frac{2ZZ_\alpha}{\hbar v}, \quad \hbar v = \hbar c \sqrt{\frac{2Q}{\mu_\alpha c^2}}. \quad (2.10)$$

For the first ho potential we use the condition that the first eigenvalue is the Q value

$$Q - V_0 = \frac{1}{2} \hbar \omega_0, \quad (2.11)$$

giving for the length ho parameter

$$b_0 = R_2 - R_0. \quad (2.12)$$

Concerning the second inverted ho potential in (2.4) we use the obvious condition

$$\frac{1}{2}\beta_1\hbar\omega_1 = \frac{1}{2}d_\alpha(\hbar\omega_1)^2 = \frac{V_B - Q}{(R_B - R_2)^2}, \quad (2.13)$$

giving the expression of the barrier frequency,

$$\hbar\omega_1 = \frac{1}{R_B - R_2} \sqrt{\frac{2V_{\text{frag}}}{d_\alpha}}, \quad (2.14)$$

and the following representation of the potential:

$$\begin{aligned} V(R) - Q &= (V_B - Q) \left[1 - \left(\frac{R_B - R}{R_B - R_2} \right)^2 \right] \\ &\equiv V_{\text{frag}}(1 - x^2), \end{aligned} \quad (2.15)$$

in terms of the fragmentation potential

$$V_{\text{frag}} = V_B - Q, \quad (2.16)$$

and dimensionless coordinate,

$$x = \frac{R_B - R}{R_B - R_2}. \quad (2.17)$$

Imposing the continuity of potential derivatives given by using Eq. (2.4) at the turning point R_2 ,

$$\hbar\omega_0\beta_0(R_2 - R_0) = \hbar\omega_1\beta_1(R_B - R_2), \quad (2.18)$$

one obtains through Eqs. (2.6), (2.12), and (2.14) the following connection between ho frequencies:

$$\begin{aligned} (\hbar\omega_0)^3 &= (\hbar\omega_1)^4 d_\alpha (R_B - R_2)^2 \\ &= \frac{4}{d_\alpha} \left(\frac{V_{\text{frag}}}{R_B - R_2} \right)^2. \end{aligned} \quad (2.19)$$

B. Decay width

We use the standard form of the decay width for decays between ground states of even-even nuclei with $J_P = J_D = 0$ in Eq. (2.1), where the angular momentum carried by the α -particle is $l = 0$ [10]

$$\Gamma_0 = \hbar v \left[\frac{f_{\text{int}}(R)}{f_{\text{ext}}(R)} \right]^2. \quad (2.20)$$

Here f_{ext} is given by the monopole irregular Coulomb wave with the WKB estimate of Eq. (A10)

$$\begin{aligned} f_{\text{ext}}(R) &= G_0(\chi, \rho) \\ &\approx \left[\frac{Q}{V_C(R) - Q} \right]^{1/4} \exp \left[\chi \left(\alpha - \frac{1}{2} \sin 2\alpha \right) \right], \end{aligned} \quad (2.21)$$

where

$$\cos^2 \alpha \equiv \frac{\rho}{\chi} = \frac{Q}{V_C(R)}. \quad (2.22)$$

Notice that the above semiclassical estimate, valid for a pure Coulomb potential, gives an error of 3–5% with respect to the exact function. At the Coulomb barrier, where $V_B \approx 0.94V_C(R_B)$, according to the second line of Eq. (A12), a change of 5% in χ corresponds to a similar variation by 5% of the irregular Coulomb function for a typical α -decay value

$\chi \sim 40$. This is the reason we used the same relation (2.21) in the barrier region (2) of the potential (2.4).

By using the expression of the internal wave function at the barrier radius (A2)

$$\begin{aligned} f_{\text{int}}(R_B) &= N_1 f_1(R_B) \\ &= N_1 \left(\frac{Q}{V_{\text{frag}}} \right)^{1/4} \exp \left(-\frac{\pi V_{\text{frag}}}{2\hbar\omega_1} \right), \end{aligned} \quad (2.23)$$

one obtains the following factorization of the decay width:

$$\Gamma_0 = \hbar v \left[\frac{f_{\text{int}}(R_B)}{f_{\text{ext}}(R_B)} \right]^2 \equiv \gamma_0^2 P_0, \quad (2.24)$$

in terms of the “reduced width,” which coincides with the squared barrier scattering amplitude

$$\gamma_0^2 = N_1^2, \quad (2.25)$$

and the “barrier penetrability,”

$$\begin{aligned} P_0 &= \hbar v \exp \left[-\frac{\pi V_{\text{frag}}}{\hbar\omega_1} - 2\chi \left(\alpha_B - \frac{1}{2} \sin 2\alpha_B \right) \right] \\ &= P_0^N P_0^C, \end{aligned} \quad (2.26)$$

proportional to the product between the nuclear and Coulomb penetrabilities. Notice that at the barrier the common factor $(Q/V_{\text{frag}})^{1/4}$, multiplying the exponential part of the external Coulomb (2.21) and internal nuclear (2.23) wave functions, simplifies in Eq. (2.24) and therefore the above relation becomes proportional to the usual penetrability integral,

$$P_0 \approx \hbar v \exp \left[-2 \int_{R_2}^{R_3} \sqrt{\frac{2\mu_\alpha}{\hbar^2} (V(R) - Q)} dR \right], \quad (2.27)$$

where R_2 and R_3 are the second and third turning points of the α -core interaction defined by the nuclear plus Coulomb barrier in Fig. 1. This expression is simpler than that given in Ref. [24], due to the approximation we made in the barrier region.

Let us also mention that the above “reduced width” introduced by us is proportional to the standard reduced width at the barrier radius [10],

$$\bar{\gamma}_0^2 = \frac{f_{\text{int}}^2(R_B)}{2d_\alpha R_B}, \quad (2.28)$$

defined by considering the standard Coulomb penetrability,

$$\bar{P}_0^C = \frac{2\rho_B}{f_{\text{ext}}^2(R_B)}, \quad (2.29)$$

in the factorization of the decay width,

$$\Gamma_0 = \bar{\gamma}_0^2 \bar{P}_0^C. \quad (2.30)$$

Thus, one obtains the following relation:

$$\log_{10} \bar{\gamma}_0^2(R_B) \sim -\frac{\pi \log_{10} e}{\hbar\omega_1} V_{\text{frag}}, \quad (2.31)$$

called in Ref. [15] the “universal law for reduced widths,” evidencing the linear dependence on the fragmentation potential (2.16) with a negative slope which is inversely proportional to the ho frequency characterizing the nuclear interaction $\hbar\omega_1$. It

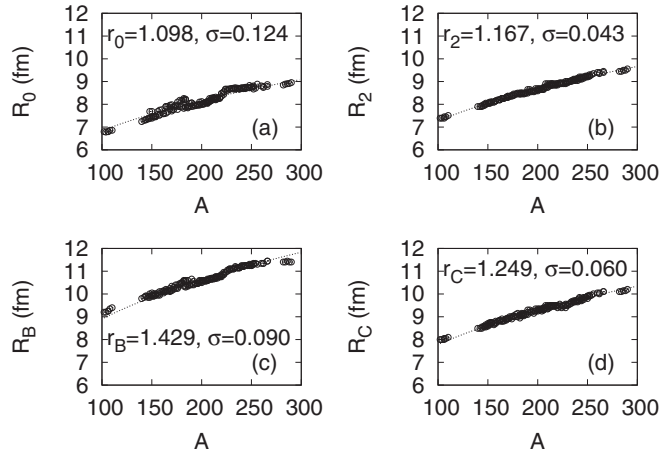


FIG. 2. Radial parameters versus mass number of the daughter even-even nucleus corresponding to the fitting relation $R_a = r_a (A^{1/3} + R_\alpha^{1/3})$ (dots) for the minimum of the ho potential r_0 (a), second turning point r_2 (b), realistic Coulomb barrier r_B (c), and schematic Coulomb barrier given by Eq. (2.4) r_C (d).

turns out that this law is fulfilled not only for α decay but also for all particle and cluster emission processes.

The generalization to transitions within odd-mass nuclei is straightforward by considering the lowest transferred angular momentum $l = |J_P - J_D|$ in the irregular Coulomb wave $G_l(\chi, \rho)$, leading to the largest barrier penetrability. For favored transitions with $J_P = J_D$, where the state of the unpaired nucleon remains unchanged during transition, one obtains the same penetrability (2.26) with $l = 0$.

III. NUMERICAL APPLICATION

A. Transitions from even-even emitters

We included in our analysis 149 even-even emitters with α -decay experimental data (decay widths and Q values) having a high degree of confidence concerning the branching ratio to the ground state [25].

The analysis by means of the potential (2.4), plotted in Fig. 1, evidenced the following parametrization of the relevant radii:

$$R_a = r_a (A^{1/3} + A_\alpha^{1/3}), \quad a = 0, 2, B, C, \quad (3.1)$$

where the values of r_a are given in Fig. 2.

By dotted curves we plotted the corresponding fitting lines. Let us stress on the fact that the small rms errors (standard deviation) with respect to these lines, $\sigma < 0.09$, suggest that we can use the fitted values of r_2 and r_B given in Fig. 2 in order to estimate the nuclear and Coulomb penetrability terms in Eq. (2.26).

Notice that the radius R_C , where the ho repulsion crosses the pure Coulomb interaction (schematic Coulomb barrier), is comparable with the geometrical touching radius, estimated by the standard relation

$$\begin{aligned} R_T &= R_N + R_\alpha = r_T (A^{1/3} + A_\alpha^{1/3}) \\ r_T &= 1.2 \text{ fm}. \end{aligned} \quad (3.2)$$

TABLE I. Regions of α emitters.

Region	Z	N	Symbol
I	$50 < Z < 82$	$50 \leq N < 82$	Open squares
II	$50 < Z < 82$	$82 \leq N < 126$	Dark squares
III	$82 \leq Z \leq 100$	$82 \leq N < 126$	Open circles
IV	$82 \leq Z \leq 100$	$N \geq 126$	Dark circles
V	$Z > 100$	$N \geq 126$	Open triangles

The nuclear radius $R_N = 1.2 A^{1/3}$, where the nuclear density diminished to about 50% of the central value, is by about 1 fm smaller than the radius defining the minimal value of the potential pocket $R_0 = 1.1 (A^{1/3} + 4^{1/3})$, where the wave function reaches its maximal value [20]. Therefore this model indeed predicts that the α cluster is mainly born in a region where the nuclear density is less than 20% (Mott density) with respect to the central value, as suggested by recent theoretical estimates [14,26].

We then analyzed the α -core interaction potential for the regions described in Table I, denoted by the corresponding symbols in the following plots. In Fig. 3(a), we plotted the Coulomb parameter χ (2.10), defining the Coulomb penetrability P_0^C , and in Fig. 3(b) the fragmentation potential (2.16) entering the nuclear penetrability P_0^N versus the neutron number. Notice the pronounced minima, especially for the fragmentation potential, corresponding to the neutron $N = 126$ and proton magic numbers $Z = 82$. Let us mention

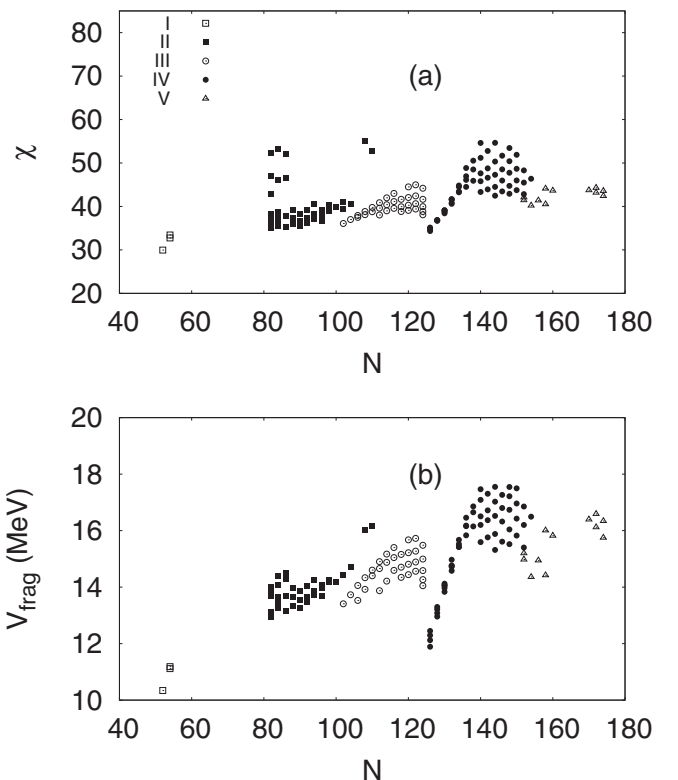


FIG. 3. Coulomb parameter χ (2.10) (a) and fragmentation potential (2.16) (b) versus the neutron number.

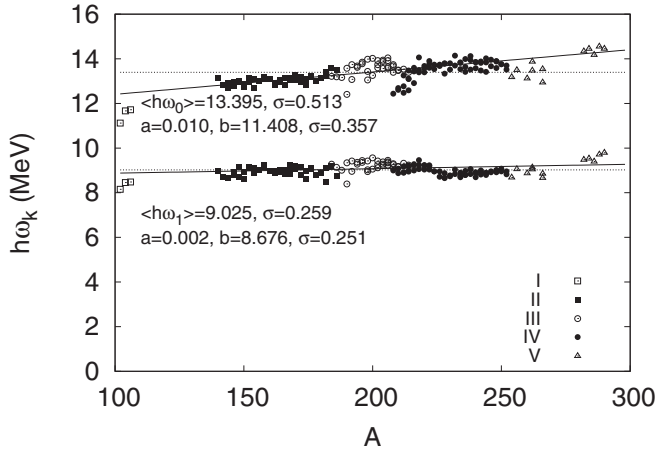


FIG. 4. The $h\omega_k$ frequencies $\hbar\omega_k$, defined by Eqs. (2.18), with $k = 0$ and (2.14) for $k = 1$ versus the mass number for even-even emitters. The parameters listed for each k are the slope, intercept, and standard deviation of the linear fit versus the mass number.

a smaller minimum, separating the regions IV and V and corresponding to the semimagic neutron number $N = 152$.

In Fig. 4 we plotted the values of $h\omega_k$ frequencies, defined by Eq. (2.18) for $k = 0$, corresponding to the internal pocket, and by Eq. (2.14) for $k = 1$, corresponding to the nuclear attraction, versus the mass number. Notice that the $h\omega$ frequency, characterizing the shape of the nuclear attraction region (1) of Eq. (2.4), has a universal value $\hbar\omega_1 \approx 9$ MeV with a small rms error $\sigma \approx 0.26$.

In Fig. 5 we estimated the length parameters b_k , defined by Eq. (2.6) for even-even emitters. Let us remark the persistence of a quasicontant behavior with respect to the mass number around the values $b_0 \approx 0.9$ fm and $b_1 \approx 1.1$ fm. In Ref. [20] we estimated values scattered in the interval $b_0 \in [0.6, 0.8]$ fm, due to the fact that we used a different procedure involving not only the matching between potentials at the second turning point R_2 but also between logarithmic derivatives of internal and external wave functions defining the resonant Gamow state.

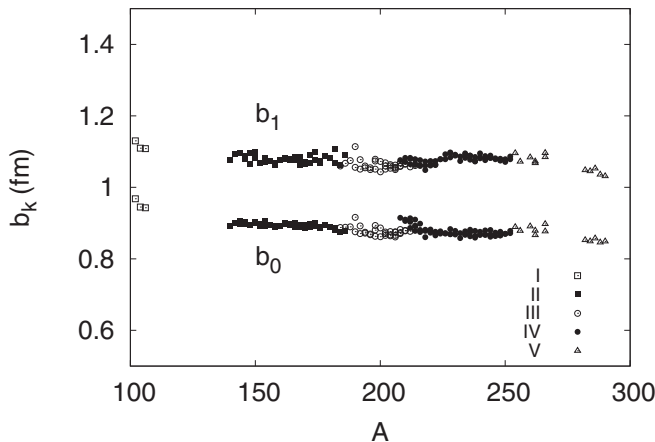


FIG. 5. The $h\omega$ length parameters b_k , defined by Eq. (2.6), versus the mass number for even-even emitters.

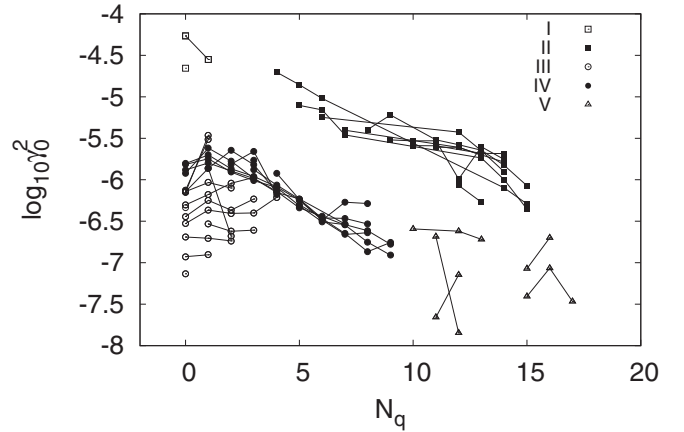


FIG. 6. The logarithm of the reduced width versus the number of α clusters above the closest doubly magic nuclei N_q for even-even emitters. The α lines connect nuclei with the same magic asymmetry $I_{\text{mag}} = n_\nu - n_\pi$.

We used the factorization (2.24) in order to extract the experimental reduced width

$$\gamma_{\text{exp}}^2 = \frac{\Gamma_{\text{exp}}}{P_0}. \quad (3.3)$$

The logarithm of this quantity was fitted by the following linear dependence:

$$\log_{10} \gamma_{\text{exp}}^2 = -(C_k N_q + A_k I_{\text{mag}} + B_k) \equiv V_\alpha, \quad (3.4)$$

where k labels the regions I–V given in Table I. We introduced the number of quartets above the closest magic number,

$$N_q = n_\pi, \quad (3.5)$$

multiplying the quartet slope C_k and the magic asymmetry,

$$I_{\text{mag}} = n_\nu - n_\pi, \quad (3.6)$$

multiplying the asymmetry slope A_k , with

$$n_\pi = \frac{Z - Z_{\text{mag}}}{2}, \quad n_\nu = \frac{N - N_{\text{mag}}}{2}, \quad (3.7)$$

these quantities being the number of proton/neutron pairs above the closest proton/neutron magic number $Z_{\text{mag}}/N_{\text{mag}}$. The lines connecting various quartet numbers $N_q = N_q^{(0)}, N_q^{(0)} + 1, \dots$ above some doubly magic nucleus plus a given magic asymmetry I_{mag} are called α lines. In Ref. [27] was evidenced a dependence of the α -decay Q value along α lines on the standard asymmetry $I = (N - Z)/A$. Let us mention here that a dependence of $\log_{10}(\Gamma_{\text{exp}})$ on the above-mentioned standard asymmetry was considered in Refs. [28–31].

In Fig. 6 we plotted the logarithm of the experimental reduced width (3.3) versus the number of quartets N_q along different α lines. The general trend, excepting region III, shows a decreasing behavior which can be explained in terms of the Pauli exclusion principle between α clusters. Our analysis revealed that this quantity has a maximal value for one cluster moving around a doubly magic nucleus. It

TABLE II. Fitted parameters of the reduced width systematics, given by Eq. (3.4) for even-even (a) and odd-mass emitters (b) in the regions defined by Table I.

k	C_k	A_k	B_k	rms error	emitters
(a) Even-even emitters					
I and II	0.105	0.033	4.682	0.154	3 + 41
III	-0.075	0.107	4.746	0.207	33
IV	0.118	0.021	5.620	0.122	60
V	0.051	0.043	6.023	0.233	12
(b) Odd-mass emitters					
IV	0.182	-0.027	5.874	0.148	21

exponentially decreases,

$$\gamma_{\text{exp}}^2(N_q) = \gamma_{\text{exp}}^2(0) 10^{-C_k N_q}, \quad (3.8)$$

as soon as more N_q clusters are added, because the Pauli exchange effect destroys the four-body correlations. The maximal reduced width above a doubly magic nucleus,

$$\gamma_{\text{exp}}^2(0) = 10^{-A_k I_{\text{mag}} - B_k}, \quad (3.9)$$

exponentially depends on the magic asymmetry I_{mag} .

We used the ansatz (3.4) in order to fit experimental reduced widths for each region defined by Table I. Let us mention here that for the superheavy region V we excluded from the fitting procedure the two points with the lowest reduced widths. The obtained parameters are given in Table II(a). Notice the similarity of C_k and A_k slope parameters for the regions I and II and IV and V, while for region III they are significantly different, due to its specific character. Here the quartet slope C_k has a similar value but with an opposite sign. Therefore, clustering increases here by approaching the neutron magic number $N_{\text{mag}} = 126$, as already suggested from the corresponding α -like chains in Fig. 6. Let us mention that this transitional region has a special “neutron hole” character, namely the number of valence neutron pairs is closer to the upper magic number $N_{\text{mag}} = 126$ than the lower one $N_{\text{mag}} = 82$. In Fig. 7(a) we plotted the dependence of the lowest quartet number versus the magic asymmetry for even-even emitters. Notice that the region III (open circles) is indeed characterized by the largest values of the magic asymmetry I_{mag} . Most α chains have positive magic asymmetries, except region II and partially region IV. Let us also emphasize the fact that all α chains start with a small number of clusters, $N_q^{(0)} \sim 0$. The superheavy region V, where $N_q^{(0)} = 10$, has a special character, suggestive of a semimagic proton number $Z_{\text{mag}} \geq 102$.

By using the parameters fitted in these regions, we plotted in Fig. 8 the logarithm of the reduced width versus the variable $V_\alpha = -(C_k N_q + A_k I_{\text{mag}} + B_k)$. This dependence is concentrated around the first bisector by covering four orders of magnitude with a small rms error $\sigma \sim 0.2$, corresponding to a mean error factor of 1.6. This plot is a clear evidence of the similar Pauli suppression of α clusters along different α lines.

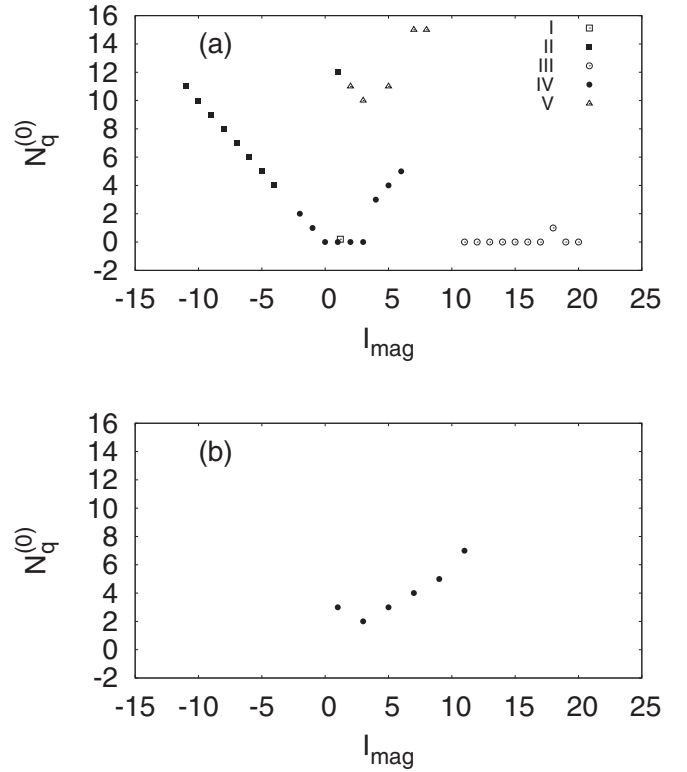


FIG. 7. The lowest quartet number $N_q^{(0)}$ versus the magic asymmetry I_{mag} , defining the α line, for even-even emitters (a) and odd-mass emitters (b). The symbols are the same as in Fig. 6.

B. Favored transitions from odd-mass emitters

We analyzed 21 favored α transitions from odd mass nuclei. These transitions are similar to those from even-even emitters, due to the fact that the state of the odd nucleon remains unchanged during the emission process. Available experimental data concerning favored transitions covers only region IV of Table I. Thus, the dependence of the Coulomb parameter and fragmentation potential is given by the

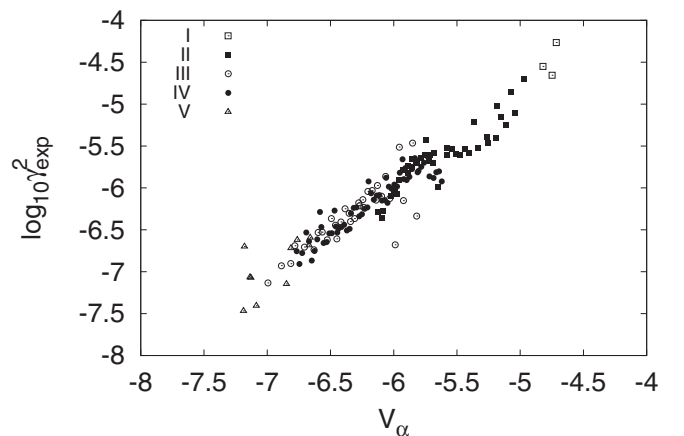


FIG. 8. Logarithm of the reduced width versus the variable V_α (3.4) for even-even emitters.

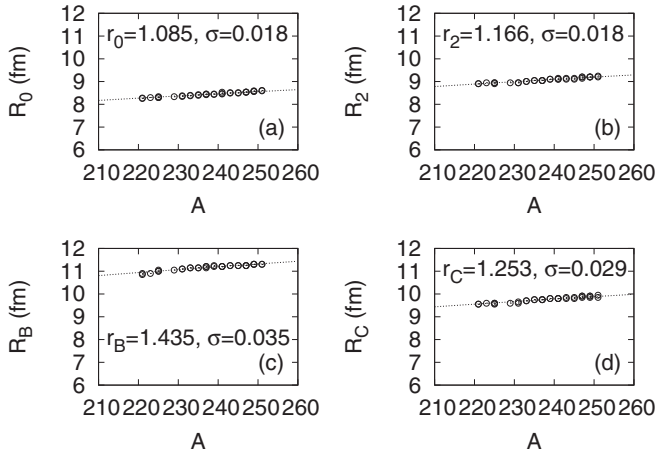


FIG. 9. Radial parameters for odd-mass emitters. The notations are the same as in Fig. 2.

corresponding neutron region (dark circles) of Figs. 3(a) and 3(b), respectively.

From Fig. 7(b) one can see that the dependence of the lowest quartet number versus the magic asymmetry, defining a given α line, is very similar to the even-even region IV in Fig. 7(a) (dark circles).

In Fig. 9 we represented radial parameters given by Eq. (3.1). Notice that they are very similar to the parameters given in Fig. 2 for even-even emitters, with smaller errors.

We obtained similar dependencies as for even-even emitters concerning ho frequencies $\hbar\omega_k$, given in Fig. 10(a), and length parameters b_k , plotted in Fig. 10(b), with $k = 0, 1$, respectively. Notice that the nuclear ho parameter has a very close value to that of the even-even case $\hbar\omega_1 \approx 9$ MeV, with a small rms error.

We used these parameters to compute the penetration factor (2.26) in order to estimate the experimental reduced width (3.3). It is plotted in Fig. 11(a) versus the number of quartets N_q calculated along different α lines. Using the fitting procedure we obtained a similar quartet slope parameter C_{IV} but a negative value of the asymmetry slope parameter A_{IV} , given in Table II(b). In Fig. 11(b) we plotted the logarithm of the reduced width versus the variable V_α (3.4). One obtains a linear dependence in both panels, similar to the even-even case.

Finally, in Fig. 12 we plotted the logarithm of the experimental decay width versus the variable $\log_{10} P_0 + V_\alpha$ for all analyzed even-even and odd-mass emitters. We obtained a straight line along the first bisector in terms of the variable V_α (3.4), depending on the quartet slope and magic asymmetry parameters.

IV. CONCLUSIONS AND PERSPECTIVES

We approximated the realistic α -core nuclear interaction, derived within the double folding procedure, by a parabolic dependence. The corresponding harmonic oscillator frequency has a quasiconstant value $\hbar\omega_1 \approx 9$ MeV for all analyzed α emitters. The penetrability through the nuclear barrier

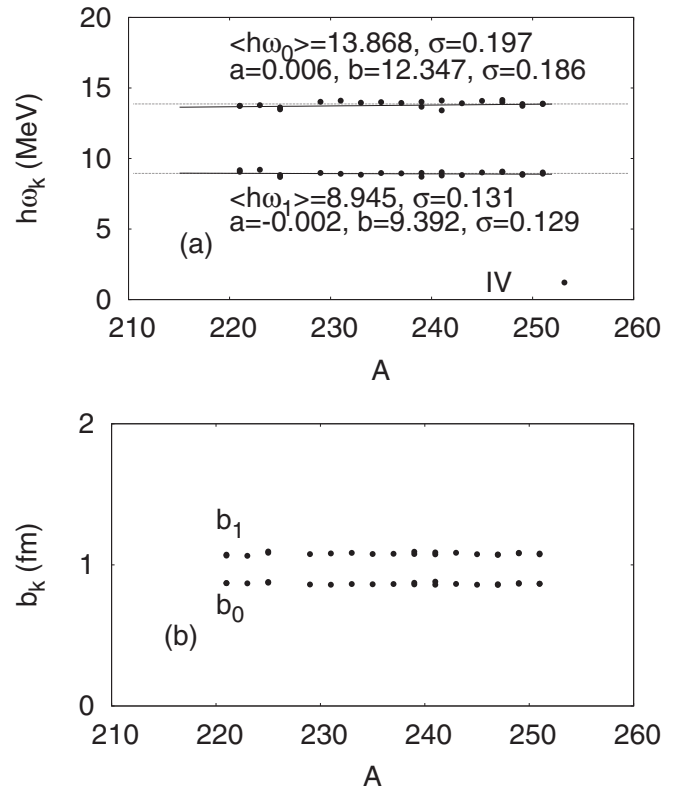


FIG. 10. (a) The ho frequencies $\hbar\omega_k$, defined by Eqs. (2.18), for $k = 0$ and (2.14) for $k = 1$ versus the mass number for odd-mass emitters. (b) The ho length parameters b_k , defined by Eq. (2.6), versus the mass number for odd-mass emitters. The parameters listed for each k are the slope, intercept, and standard deviation of the linear fit versus the mass number.

depends on the ratio between the fragmentation potential and this ho frequency.

Let us stress that our purpose was not to provide yet another empirical systematics of the α -decay width versus some parameters, like in Fig. 12, but mainly to analyze the physical similarities of the reduced width along α lines defined by the magic neutron-proton asymmetry parameter $I_{\text{mag}} = n_\nu - n_\pi$, in terms of the quartet slope C_k and asymmetry slope A_k . We obtained an important result, namely that all regions defined by proton $Z_{\text{mag}} = 50, 82$ and neutron magic numbers $N_{\text{mag}} = 50, 82, 126$ have similar parameters, except for a special region, region III, defined in Table I. Thus, we have shown that the logarithm of the reduced width for even-even emitters linearly decreases along various α lines with respect to the number of clusters above doubly magic nuclei except for region III, where the number of proton valence pairs is much smaller than the number of neutron valence pairs. We also evidenced that the logarithm of the reduced width linearly depends on the magic asymmetry I_{mag} for even-even, as well as for odd-mass emitters.

Our next goal is to explain the behavior of the preformation amplitude, proportional to the square root of the reduced width given by Eqs. (3.8) and (3.9), in terms of the overlap between the parent and the antisymmetrized product between

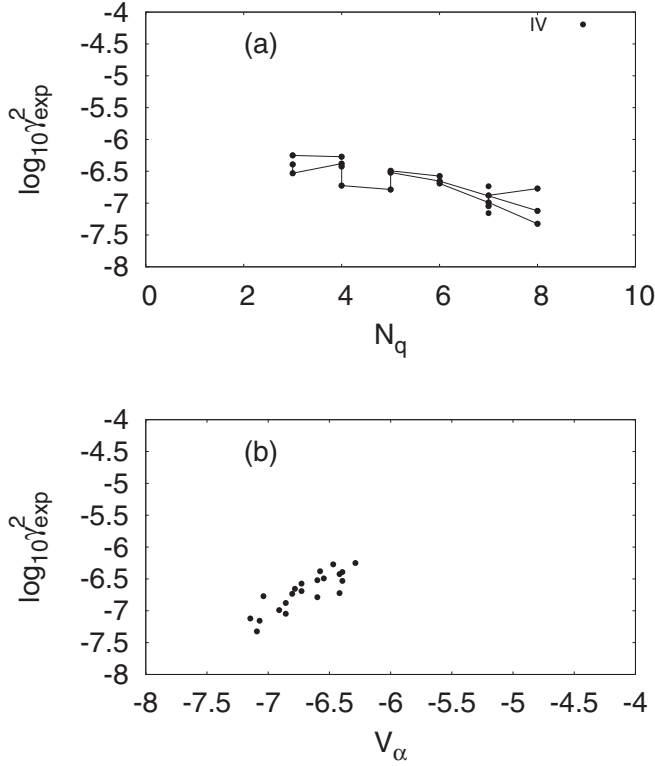


FIG. 11. Logarithm of the reduced width versus the number of α clusters N_q (a) and versus the variable V_α (3.4) and (b) for odd-mass emitters.

the daughter and internal α -particle wave functions [10],

$$\gamma_0 \sim \langle \Psi_P | \mathcal{A}(\Psi_D \psi_\alpha) \rangle. \quad (4.1)$$

We will use simple microscopic quartetting models taking into account the Pauli exclusion principle between fermionic pairs [32–34].

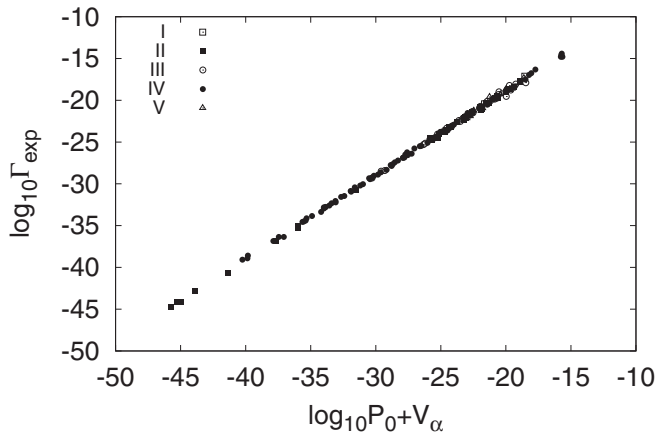


FIG. 12. Logarithm of the experimental decay width versus the variable $\log_{10} P_0 + V_\alpha$ for all analyzed emitters.

ACKNOWLEDGMENTS

This work was supported by the grant of the Romanian Ministry of Education and Research (Grant No. PN-18090101/2019-2021).

APPENDIX: SEMICLASSICAL ESTIMATE OF WAVE FUNCTIONS

1. Internal barrier

The barrier in region (1) of the nuclear interaction (2.4) can be approximated with good accuracy by a parabolic dependence. The solution of the Schrödinger equation for the inverted harmonic oscillator has an analytical form in terms of the confluent hypergeometric function [35], but in our case one can obtain the following simple WKB ansatz of the decreasing solution

$$\begin{aligned} f_1(R) &\approx \left[\frac{V(R)}{Q} - 1 \right]^{-1/4} \exp \left[- \int_{R_2}^R \sqrt{\frac{2\mu_\alpha}{\hbar^2} (V(R) - Q)} dR \right] \\ &= \left[\frac{V_{\text{frag}}}{Q} (1 - x^2) \right]^{-1/4} \\ &\quad \times \exp \left[- \frac{V_{\text{frag}}}{\hbar\omega_1} \left(\frac{\pi}{2} - \sin^{-1} x - x\sqrt{1 - x^2} \right) \right] \\ &\equiv f_1(R_B) F \left(\frac{V_{\text{frag}}}{\hbar\omega_1}, x \right), \end{aligned} \quad (A1)$$

in terms of the dimensionless coordinate (2.17).

Here we introduced the WKB function at the barrier $R = R_B$ ($x = 0$)

$$f_1(R_B) = \left(\frac{Q}{V_{\text{frag}}} \right)^{1/4} \exp \left(- \frac{\pi V_{\text{frag}}}{2\hbar\omega_1} \right), \quad (A2)$$

and the universal function

$$F(a, x) \equiv (1 - x^2)^{-1/4} \exp[a(\sin^{-1} x + x\sqrt{1 - x^2})], \quad (A3)$$

depending on the dimensionless parameter,

$$a = \frac{V_{\text{frag}}}{\hbar\omega_1}. \quad (A4)$$

Let us mention that the function $\ln F(a, x)$ versus x , given in Fig. 13 by solid lines for realistic values $a = 1, 1.5, 2,$ and 2.5 , (see Fig. 3) can be approximated in the interval $x \in [0, 0.9]$ by a linear dependence (dashed lines), i.e.,

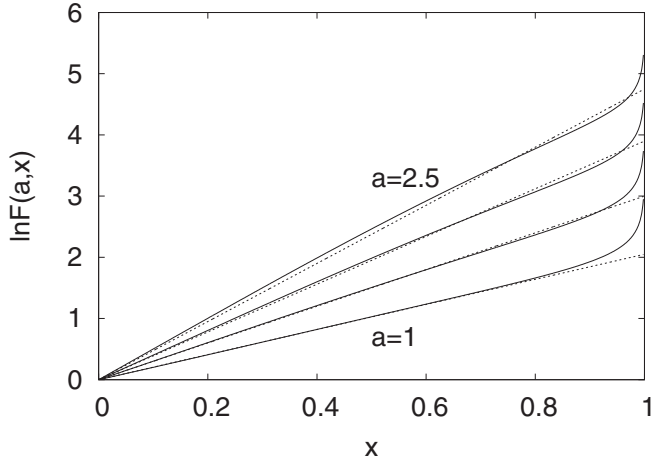
$$F(a, x) \approx e^{dx}, \quad d \approx a(2.15 - 0.1a), \quad (A5)$$

thus obtaining the extrapolated values at the second turning point $R = R_2$ ($x = 1$).

Notice that the wave function in the pocket region (0) of the potential defined by Eq. (1) is given by a shifted Gaussian,

$$f_0(R) = N_0 \left(\frac{\beta_0}{\pi} \right)^{1/4} e^{-\frac{1}{2}\beta_0(R-R_0)^2}, \quad (A6)$$

and the normalization factor N_0 can be determined in terms of the barrier scattering amplitude N_1 by matching it with the


 FIG. 13. The function $\ln F(a, x)$ versus x for $a = 1, 1.5, 2,$ and 2.5 .

wave function in the barrier region (1),

$$f_{\text{int}}(R) = N_1 f_1(R_B) F\left(\frac{V_{\text{frag}}}{\hbar\omega_1}, x\right), \quad (\text{A7})$$

at the second turning point $x = 1$. By considering its exponential approximation (A5),

$$f_0(R_2) = N_0 \left(\frac{\beta_0}{\pi}\right)^{1/4} e^{-1/2} = N_1 f_1(R_B) e^d, \quad (\text{A8})$$

one obtains the following expression:

$$N_0 = N_1 f_1(R_B) \left(\frac{\pi}{\beta_0}\right)^{1/4} e^{d+1/2}. \quad (\text{A9})$$

2. External barrier

The WKB estimate of the monopole irregular Coulomb function in terms of the reduced radius, valid for the pure Coulombian region (3) of the potential (2.4), is given by [10]

$$G_0(\chi, \rho) \approx (\cot \alpha)^{1/2} \exp\left[\chi\left(\alpha - \frac{1}{2} \sin 2\alpha\right)\right], \quad (\text{A10})$$

where

$$\begin{aligned} \cos^2 \alpha &= \frac{\rho}{\chi} = \frac{Q}{V_C(R)} \\ (\cot \alpha)^{1/2} &= \left[\frac{Q}{V_C(R) - Q}\right]^{1/4}. \end{aligned} \quad (\text{A11})$$

Concerning the pre-exponential factor, at the barrier R_B one obviously obtains the same factor in front of the exponent as for the internal wave function (A2). For its logarithmic derivatives one obtains

$$\begin{aligned} \frac{1}{G_0} \frac{dG_0}{d\rho} &= \frac{1}{\chi \sin 2\alpha} \left[\frac{1}{\sin 2\alpha} - \chi(1 - \cos 2\alpha) - \frac{l(l+1)}{\chi \cos^2 \alpha} \right] \\ \frac{1}{G_0} \frac{dG_0}{d\chi} &= -\frac{1}{4\chi \sin^2 \alpha} + \alpha - \frac{1}{2} \sin 2\alpha \\ &\quad + \frac{1}{2}(1 - \cos 2\alpha) \cot \alpha. \end{aligned} \quad (\text{A12})$$

Let us mention in this context that in the pure Coulomb region (3) of Eq. (2.4) the relative error of the approximation for the relation (A10) is less than 5%, and the error of the derivatives (A12) is less than 1% with respect to the corresponding exact solution. It turns out that the irregular function (A10) gives also a very good approximation, with an error less than 5%, with respect to the exact solution at the Coulomb barrier where $V(R_B) \sim 0.94V_C(R_B)$.

- [1] P. Schuck, Y. Funaki, H. Horiuchi, G. Röpke, A. Tohsaki, and T. Yamada, *Phys. Scr.* **91**, 123001 (2016).
- [2] A. Tohsaki, H. Horiuchi, P. Schuck, and G. Röpke, *Rev. Mod. Phys.* **89**, 011002 (2017).
- [3] W. von Oertzen, M. Freer, and Y. Kanada-Enyo, *Phys. Rep.* **432**, 43 (2006).
- [4] Y. K. Gambhir, P. Ring, and P. Schuck, *Phys. Rev. Lett.* **51**, 1235 (1983).
- [5] B. Buck, A. C. Merchant, and S. M. Perez, *Phys. Rev. C* **51**, 559 (1995).
- [6] D. S. Delion and J. Suhonen, *Phys. Rev. C* **61**, 024304 (2000).
- [7] G. Gamow, *Z. Phys.* **51**, 204 (1928).
- [8] E. U. Condon and R. W. Gurney, *Nature* **122**, 439 (1928).
- [9] A. M. Lane and R. G. Thomas, *Rev. Mod. Phys.* **30**, 257 (1958).
- [10] D. S. Delion, *Theory of Particle and Cluster Emission* (Springer-Verlag, Berlin, 2010).
- [11] K. Varga, R. G. Lovas, and R. J. Liotta, *Phys. Rev. Lett.* **69**, 37 (1992); *Nucl. Phys. A* **550**, 421 (1992).
- [12] D. S. Delion and R. J. Liotta, *Phys. Rev. C* **87**, 041302(R) (2013).
- [13] G. Röpke, A. Schnell, P. Schuck, and P. Nozieres, *Phys. Rev. Lett.* **80**, 3177 (1998).
- [14] G. Röpke, P. Schuck, Y. Funaki, H. Horiuchi, Z. Ren, A. Tohsaki, C. Xu, T. Yamada, and B. Zhou, *Phys. Rev. C* **90**, 034304 (2014).
- [15] D. S. Delion, *Phys. Rev. C* **80**, 024310 (2009).
- [16] D. S. Delion and A. Dumitrescu, *At. Data Nucl. Data Tables* **101**, 1 (2015).
- [17] L. F. Canto and D. M. Brink, *Nucl. Phys. A* **279**, 85 (1977).
- [18] T. Fließbach and H. Walliser, *Nucl. Phys. A* **377**, 84 (1982).
- [19] R. G. Lovas, R. J. Liotta, A. Insolia, K. Varga, and D. S. Delion, *Phys. Rep.* **294**, 265 (1998).
- [20] D. S. Delion, A. Dumitrescu, and V. V. Baran, *Phys. Rev. C* **97**, 064303 (2018).
- [21] G. Bertsch, J. Borysowicz, H. McManus, and W. G. Love, *Nucl. Phys. A* **284**, 399 (1977).
- [22] G. R. Satchler and W. G. Love, *Phys. Rep.* **55**, 183 (1979).
- [23] F. Cârstoiu and R. J. Lombard, *Ann. Phys. (NY)* **217**, 279 (1992).
- [24] L. L. Li, S. G. Zhou, E. G. Zhao, and W. Scheid, *Int. J. Mod. Phys. E* **19**, 359 (2010).
- [25] *Evaluated Nuclear Structure Data Files* of the Brookhaven National Laboratory, <http://www.nndc.bnl.gov/ensdf/>.

- [26] S. Yang, C. Xu, G. Röpke, P. Schuck, Z. Ren, Y. Funaki, H. Horiuchi, A. Tohsaki, T. Yamada, and B. Zhou, *Phys. Rev. C* **101**, 024316 (2020).
- [27] G. Dussel, E. Caurier, and A. P. Zuker, *At. Data Nucl. Data Tables* **39**, 205 (1988).
- [28] Z. Ren, C. Xu, and Z. Wang, *Phys. Rev. C* **70**, 034304 (2004).
- [29] G. Royer, *Nucl. Phys. A* **848**, 279 (2010).
- [30] D. T. Akrawy and D. N. Poenaru, *J. Phys. G* **44**, 105105 (2017).
- [31] D. T. Akrawy and A. H. Ahmed, *Int. J. Mod. Phys. E* **27**, 1850068 (2018).
- [32] D. S. Delion, G. G. Dussel, and R. J. Liotta, *Rom. J. Phys.* **47**, 97 (2002).
- [33] V. V. Baran, D. S. Delion, and S. Dolteanu, *Phys. Rev. C* **100**, 034326 (2019).
- [34] V. V. Baran and D. S. Delion, *Phys. Lett. B* **805**, 135462 (2020).
- [35] D. Bermudez and D. J. Fernández, *Ann. Phys.* **333**, 290 (2013).